

# Insect abundance over Chinese rice fields in relation to environmental parameters, studied with a polarization-sensitive CW near-IR lidar system

Shiming Zhu<sup>1</sup> · Elin Malmqvist<sup>2</sup> · Wansha Li<sup>1</sup> · Samuel Jansson<sup>2</sup> · Yiyun Li<sup>1</sup> · Zheng Duan<sup>1</sup> · Katarina Svanberg<sup>1,3</sup> · Hongqiang Feng<sup>4</sup> · Ziwei Song<sup>5</sup> · Guangyu Zhao<sup>1,2</sup> · Mikkel Brydegaard<sup>2,6,7</sup> · Sune Svanberg<sup>1,3,8</sup>

Received: 25 February 2017 / Accepted: 26 June 2017 / Published online: 10 July 2017  
© The Author(s) 2017. This article is an open access publication

**Abstract** Effective monitoring of flying insects is of major societal importance in view of the role of insects as indispensable pollinators, destructive disease vectors and economically devastating agricultural pests. The present paper reports on monitoring of flying agricultural pests using a continuous-wave lidar system in a rice-field location in Southern China. Using a Scheimpflug arrangement, range resolution over several 100 m long observational paths was achieved. The system operates with two perpendicularly polarized near-infrared lasers, which are activated intermittently, and back-scattered radiation from insects was recorded by a linear array detector placed after a linear polarizer. Our polarization sensitive system was used to monitor the flying insect diurnal activity and also the influence of changes in weather conditions, e.g., the occurrence of rain. Activity strongly peaked at dusk and rose again, although to a lower extent, just before dawn. At the onset of rainfall, a strong increase in insect counts occurred which

was interpreted as the rain-induced bringing down of high-altitude migrant insects.

## 1 Introduction

A CW lidar (light detection and ranging) system was used to study the abundance of flying insects over a rice-field location in Southern China, with particular emphasis on diurnal variations and the influence of rainfall. The system was arranged to be sensitive to the depolarization properties of objects and organisms encountered by the laser beam, which propagated a few meters above ground. Two laser transects were set up: the first one (July 8–13) covered 513 m over rice fields treated with pesticides, whereas the second one (July 14–16) extended for 208 m over untreated fields.

Remote sensing methods for monitoring the flying fauna have been developed successively. Remote sensing of birds based on radar systems emerged in the latter part of the twentieth century and became more and more refined [1], and as the detection limit was improved to monitor flying

This article is part of the topical collection “Field Laser Applications in Industry and Research” guest edited by Francesco D’Amato, Erik Kerstel, and Alan Fried.

✉ Sune Svanberg  
Sune.Svanberg@fysik.lth.se

<sup>1</sup> Center for Optical and Electromagnetic Research, South China Academy of Advanced Optoelectronics, South China Normal University, University City Campus, Guangzhou 510006, China

<sup>2</sup> Combustion Physics Division, Department of Physics, Lund University, P.O. Box 118, 221 00 Lund, Sweden

<sup>3</sup> Lund Laser Centre, Lund University, P.O. Box 118, 221 00 Lund, Sweden

<sup>4</sup> International Joint Research Laboratory for Crop Protection in Henan, Institute for Plant Protection, Henan Academy of Agricultural Sciences, Zhengzhou 450002, China

<sup>5</sup> Guangdong Provincial Key Laboratory of High Technology for Plant Protection/Plant Protection Research Institute, Guangdong Academy of Agricultural Sciences, 7, Jinying Road, Tianhe District, Guangzhou 510640, China

<sup>6</sup> Department of Biology, Centre for Animal Movement Research, Lund University, 223 62 Lund, Sweden

<sup>7</sup> Norsk Elektro Optikk A/S, Prost Stabels Vei 22, 2019 Skedsmokorset, Norway

<sup>8</sup> Atomic Physics Division, Department of Physics, Lund University, P.O. Box 118, 221 00 Lund, Sweden

insects, even tiny ones with a body length of a few millimeters came into the observation capability of entomologists [2–5]. However, entomological radars still have limitations, e.g., lack of spectroscopic signatures, and difficulties in close-to-the-ground applications. A first optical entomological lidar monitoring scheme was developed by Shaw et al. and was refined by Carlsten et al. at the Montana State University [6, 7], where trained honey bees were used to detect hidden explosives. Researchers from Lund University, Sweden, first engaged in lidar insect monitoring about 8 years ago, and have used both pulsed and CW lidar systems [8–11]. A passive, so-called dark-field insect remote sensing optical method was also developed, which uses ambient radiation [12], a method which also was implemented by the South China Normal University group [13, 14]. A particularly promising new approach, using a combination of a CW laser and a linear array detector attached to a detection telescope in a so-called Scheimpflug arrangement [15], has been developed [11]. This allows for a low-cost, yet very effective way of sensing flying insects over long measurement paths. We have used such a system operating at 808 nm in the near-IR spectral region, and adapted it for polarization sensitive detection. Using two identical linearly polarized lasers, where one had its polarization plane rotated by 90° by using a  $\lambda/2$  plate, and employing a common detector preceded by a linear polarizer, the system became sensitive to target properties related to depolarization. The depolarization ratio is associated with glossiness and microstructure of the target. A joint field experiment, mostly related to rice cultivation, with participation of scientists from China and Sweden, was arranged just north of Guangzhou in Southern China during a very hot summer period, July 8–16, 2016.

An experimental farm of the Plant Protection Research Institute, Guangdong Academy of Agricultural Sciences (GAAS) was chosen for the experiment. It is located at 113.42 E, 23.42 N, 5 km south of the Tropic of Cancer and 29 m above sea level. This is a Southern sub-tropical monsoon area with average annual temperature of 20–22 °C, a relative humidity of 77%, and a rainfall of 1980 mm and sunlight time of 1750 h over a year. The sunrise and sunset times during the experiment days were around 5:50 a.m. and 7:15 p.m., respectively, and the mid-day sun transit time was around 12:33 Beijing time.

The atmospheric fauna consists of insects, birds and bats. Besides the availability of vegetation on which agricultural pests feed, their activity patterns are affected by several natural factors. The most important one is the light level stemming from the sun radiation. Many other environmental parameters also closely correlate to the sunlight level. The activity patterns of all organisms have temporal niches related to the true sun time. Many insects are nocturnal and are hidden in bushes and grass at daytime for

protection against predators, and leave the brighter period to birds and a few diurnal insects.

Temperature is another important factor for animals. In temperate areas, most insects are only active in the summer, and their behaviors vary according to temperature; e.g., the wing-beat frequencies of insects are temperature dependent. In very hot weather, insects are threatened from drying out, and relative humidity is then of importance. Most insects overwinter in diapause form when the weather gets too cold.

An overview over the experimental farm area, with the lidar optical monitoring paths indicated, is shown in Fig. 1. The longer path (513 m) is over fields, mostly with rice but also some tobacco, where pesticides have been used for controlling agricultural pests, while the shorter, perpendicular path (208 m) is over non-treated areas. The present paper only deals with data from the longer path. The insert shows some representative rice agricultural pest insects with Latin names. The interrogating laser beam was directed at a height of 3–5 m above the ground and was terminated at diffuse low-reflectance, black neoprene foam sheets on screens of a size of about 1 m<sup>2</sup>. The system is not eye safe, but eye safety was assured by the geometrical arrangement and constant surveillance of the measurement area. The CW lidar system described below was installed in a small guard hut with appropriate windows as shown in Fig. 2a, while the beam termination, as viewed during nighttime conditions by a CMOS camera (sensitive at 808 nm) which was attached to the system surveillance/overview telescope, is shown in Fig. 2b.

## 2 System description

The CW lidar system used in the present experiments is described in detail in [16]. Here, a brief description will be given with reference to Fig. 3. We use a so-called Scheimpflug arrangement [11], where range resolution can be achieved, in spite of not using a pulsed laser system as in customary systems [9, 10, 17]. The transmitted laser beam is observed by a receiving telescope, separated by a short distance from the transmitting telescope, and a linear array detector in a tilted position observes the back-scattered light, so that close-range, as well as far-range locations can be recorded in focus simultaneously. It is well known that in a normal camera the lens needs to be placed further away from the detector for close-range objects, while for far-away objects the lens is placed closer to the detector. When performing early air-borne surveillance photography, Theodor Scheimpflug realized [15] that sharp imaging could be achieved for a forward-looking camera by appropriately tilting the photographic film to compensate for different distances. The Scheimpflug lidar [11] basically

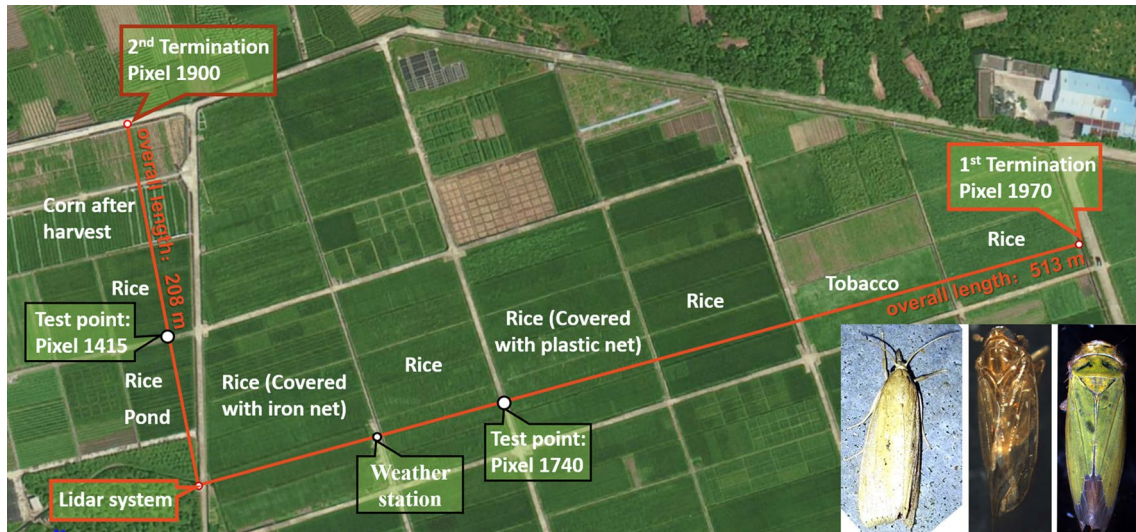


**Fig. 1** Overview of the experimental site with rice fields at the Agricultural Plant Protection Experimental Facility of the Guangdong Academy of Agricultural Sciences. Crop varieties are indicated. Two measurement paths and the position of the weather station are shown. *Pixel numbers* indicated correspond to the target location on

the linear sensor array, with a strongly non-linear range dependence as typical for a Scheimpflug arrangement. Three agricultural pest insects pertinent to rice - the striped stem borer *Chilo suppressalis*, the rice brown plant hopper *Nilaparvata lugens*, and the rice leaf hopper *Nephotettix bipunctatus* - are inserted, from left to right

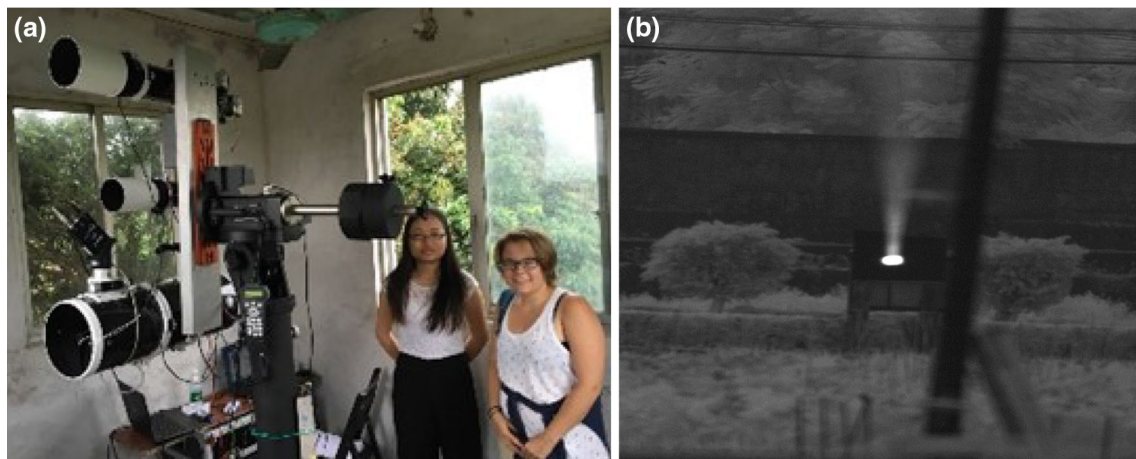


**Fig. 2 a** Photograph of the CW lidar remote sensing system, installed in a guard hut, with system transmitting telescope on top and receiving telescope below. The linear array detector, mounted at an angle to the receiving telescope as specified by the Scheimpflug condition, is also seen. **b** Near-IR picture of the long-path termination area, also showing atmospheric back-scattering of the laser beam,

which is observed slightly from below by the third, surveillance, telescope placed in between the two larger telescopes shown in (a). The leaning structure across the picture is the electric pole located at the test point indicated in Fig. 1, where nighttime UV light trapping of insects was performed. These aspects will be reported elsewhere

operates on the same principles, and there are well-defined geometrical relations between telescope separation, receiving telescope focal length and tilt angles [18, 19]. Range resolution is high at close range while intrinsically low at far distance, where ultimately all locations fall on the same detector pixel [19]. A consequence of this is that the detected return intensities for a uniform atmosphere are basically the same for all pixels, while a customary pulsed

lidar system exhibits an inverse range-squared dependence. There are several attractive features with this arrangement, such as reduced cost, weight and complexity, while allowing a high data sampling rate (See, e.g., [11, 19–21]). The beam-transmitting telescope is a 150 mm diameter, 600 mm focal length Galilean refractor (SkyWatcher Startravel), while the receiving telescope has 200 mm diameter and 800 mm focal length in a reflective Newtonian

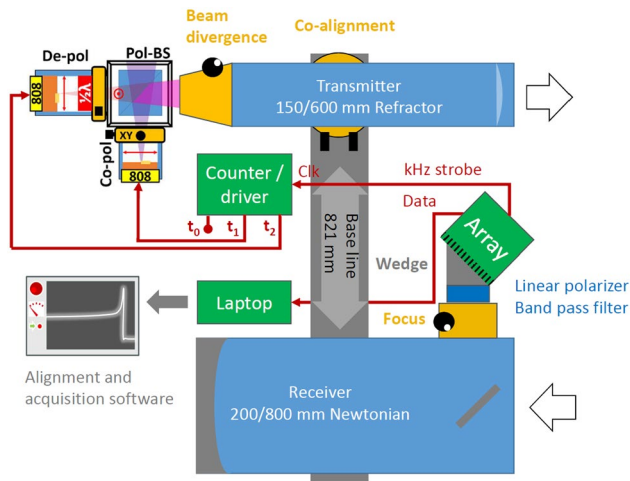


**Fig. 3** Layout of the CW Scheimpflug arrangement lidar system used in the experiment. The transmission and receiving telescopes are mounted with a small angle between them in a bi-static lidar arrangement, where range resolution can be geometrically achieved, when the scattering in the transmitted CW laser beam is observed by the tilted linear array detector. Shown in exaggerated size is the arrangement where two perpendicularly linearly polarized laser beams are combined in a prismatic beam splitter to be intermittently transmitted to generate range-resolved signals on the array detector, which is positioned behind a linear polarizer. The tilt angle is determined by the Scheimpflug condition, to compensate for the movement of the telescope focus with range

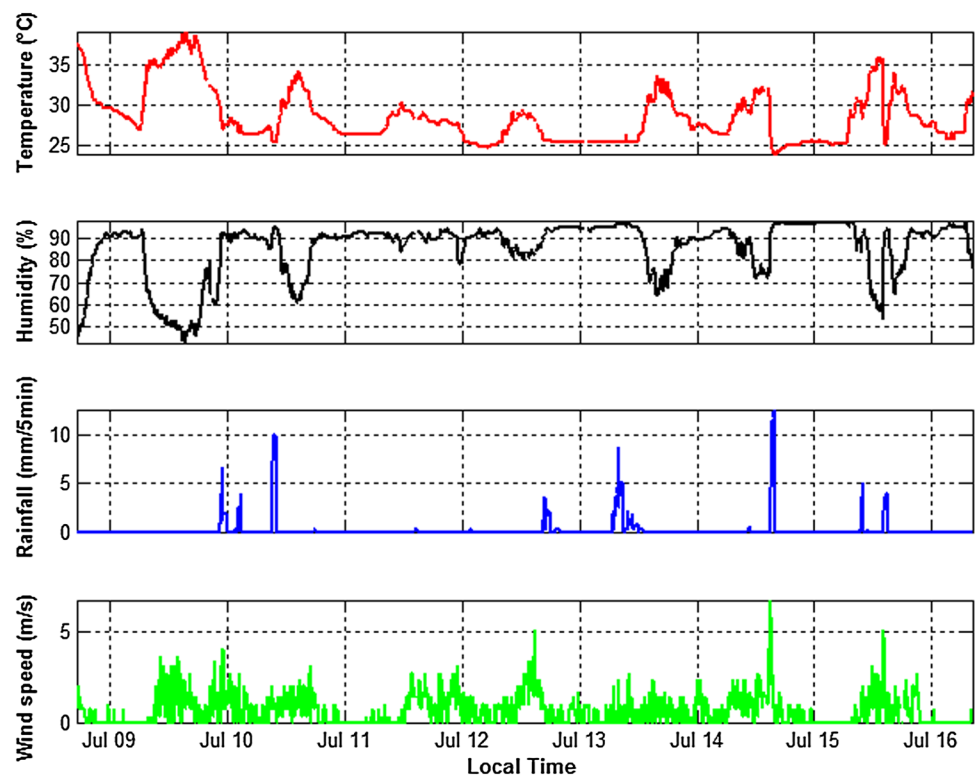
arrangement (SkyWatcher Quattro). The distance between the optical axes is 821 mm.

The telescopes are readily available amateur astronomy units. We use two linearly polarized 808 nm semiconductor lasers, each with 3.2 W nominal output. The transmitted beam is typically 15 cm wide and 5 cm high, and at a range of half a km typically 15–20 cm wide but still about 5 cm high. We use a 2048 pixel CMOS linear array detector with a maximum line rate of 4 kHz. The two lasers are sequentially activated by a driver unit, followed by an equally long period of background recording; all accomplished in 1 ms, and with every signal integration lasting 0.3 ms. The detector is preceded by a band-pass filter with a full-width at half maximum of 10 nm, and a linear polarizer; see Fig. 3. The possibility of polarization sensitive detection is a novel aspect of the present system compared to earlier implementations.

### 3 Measurements and results

Measurements were performed around the clock during the measurement campaign. Since we particularly focus on the influence of environmental parameters, weather conditions were monitored by a weather station, located as indicated in Fig. 1. Temperature, humidity, rainfall and wind speed throughout the measurement period are shown in Fig. 4.

**Fig. 4** Temperature, relative humidity (RH), rainfall and wind speed during nearly 200 h of measurements. Stable levels of temperature and RH are always observed during the nighttime hours between 0:00 to 5:00. The two weather factor curves actually mirror each other in behavior



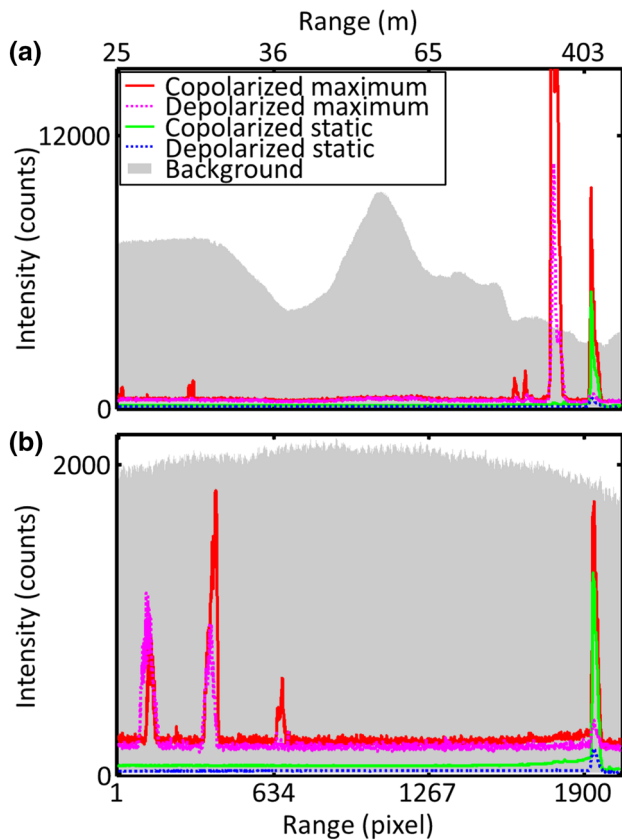


**Fig. 5** Representations of 10 s of signal from the detector array, recorded in different measurement conditions. The temporal median is representative of the static signal during the time window, arising from the backscatter in air. Through multiplexing, the signal is decomposed into co-polarized, depolarized and background, enabling quantification of the scattering properties of air in the static signal, while organisms and objects transiting the laser beam appear in the maximum signal. The laser beam is terminated at a distance of 513 m, corresponding to pixel 1970. The *horizontal scale* is linear in detector pixel numbers, but highly non-linear in range, as inherent in the Scheimpflug approach. **a** Daytime recording from 10:14 on July 9, with a high optical background. A number of smaller organisms appear in the 10 s time window, as well as a larger one. The observations can be assessed through the depolarization properties of their bodies and wings, and wing-beat modulation spectroscopy has been demonstrated for target classification. **b** Nighttime recording from 03:19 on July 9, with a low optical background. A few smaller organisms appear in this 10 s time window, with signal intensities comparable to the smaller organisms in **a**. The background level at daytime is clearly much higher compared to nighttime, and varying, reflecting non-uniform cloud coverage and spatially non-uniform ground back reflection

To exemplify the raw data obtained with the present system we show in Fig. 5 the signal read out from the array detector in day- and nighttime recordings. We notice the non-linear range scale which is typical for a Scheimpflug system. Both curves display a strong back-scattering signal from the black termination and the expected different levels of daytime background

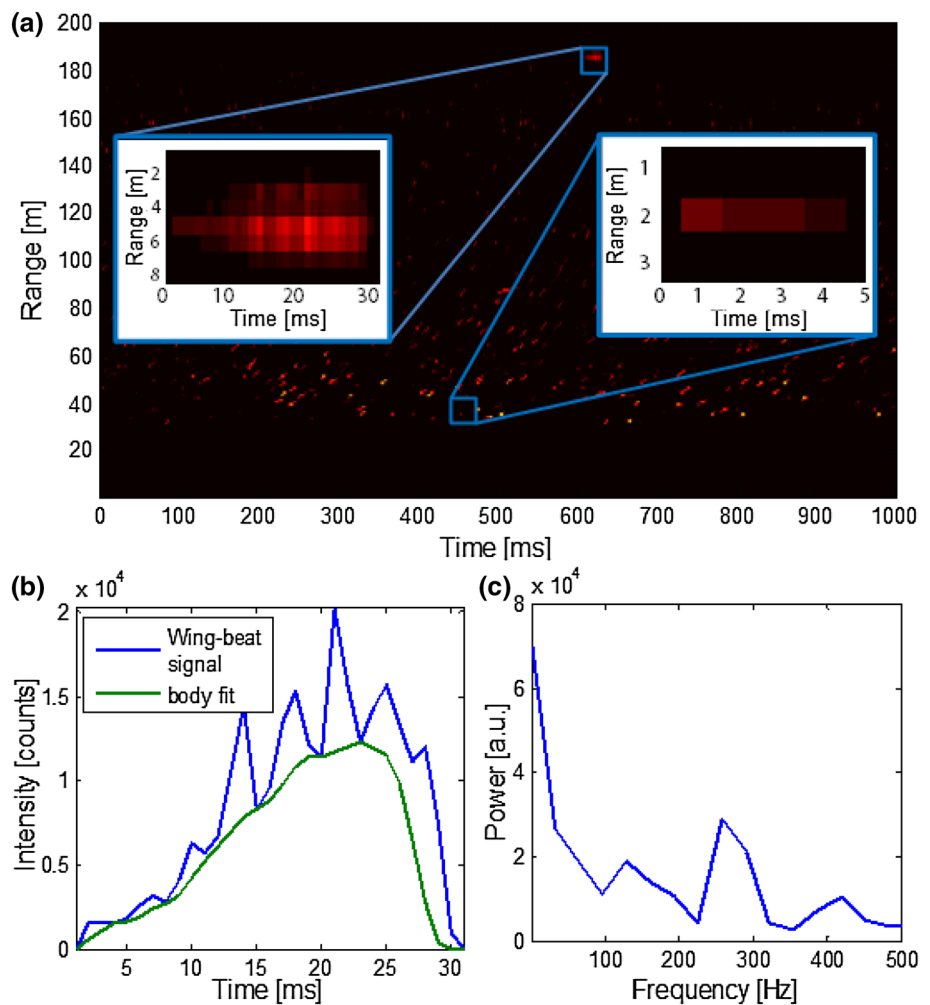
signal unrelated to the laser beam. Sharp spikes represent insects or birds crossing the laser beam, of a typical diameter of 20 cm and causing enhanced back-scattering. The strength of the echoes recorded clearly is related to the size of the object crossing, even if a large object passing in the outer part of the beam would lead to a reduced signal. The system sensitivity is range dependent, and can be calibrated by swinging a string through the laser beam at different locations along the beam path.

A raw data overview of the three first days of the field experiment is shown in Fig. 6, including rainfall, aero-fauna activity and background light level. Rain gives rise to a large amount of observations, which makes data processing extremely computationally heavy. To give an indication of the amount of sparse particles transiting the laser beam, including both aero-fauna and rain, the amount of data pixels in each 10-s time window exceeding a set noise level is plotted for the co-polarization data. There is a clear increase in pixels exceeding the threshold during dawn and dusk rush hours, when birds and bats benefit from the large availability of flying insects. Occasional rain showers also cause a large increase. A localized peak coinciding with switching on the light of a zenith pointing strong search light crossing the laser beam path is observed on one nighttime occasion. Signals occur on a static background level, which strongly varies between daytime and nighttime.

It is particularly challenging to distinguish between insects and raindrops, and to appropriately analyze the echo spikes [20, 21]. The recordings in Fig. 5 were taken for no-rain conditions, where all spikes are clearly due to flying fauna. However, for general weather conditions, raw data contain both types of events, as illustrated in Fig. 6. Rain-drop observations can be suppressed by observing that the corresponding spikes have a considerably shorter transit time through the probe volume, in our case less than 8 ms, corresponding to a falling speed of about 10 m/s. We illustrate this possibility of discrimination in Fig. 7, which is a 1-s Range/Time map where sharp temporal signals are shown at various ranges. An insect passing the beam during 30 ms is shown displaying wing-beats with the Fourier transform yielding 130 Hz as the fundamental frequency and also displaying higher harmonics. In contrast, a raindrop passes the beam in 4 ms and does not display any oscillation. The raindrops can be excluded from the data by image erosion, an image processing operation, where a certain number of pixels in a brighter part of an image are replaced with the surrounding pixel values. For a small enough bright part the whole structure then disappears, while a larger structure is “eroded” at the edges. Then, the process can be reversed by the operation “dilation”, when the structure is again dressed up till the original shape. For the spot that first disappeared, no kernel to dilate on exists, so it is permanently eliminated.



**Fig. 7** A typical Range-Time map of one second recordings is shown in (a). In the upper part, an insect flying in the rain gives rise to an oscillatory signal of about 30 ms duration, as enhanced in the expanded panel to the left. This oscillatory signal is shown in the time domain in (b). The power spectrum of this signal is obtained through a fast Fourier transform (FFT) of the signal into the temporal domain, and is shown in (c) to reveal a 130 Hz wing-beat frequency and overtones. In contrast, a typical raindrop passing the beam in about 4 ms is indicated in the lower part of (a) and also shown in detail in the expanded panel to the right



The distribution of rainfall is shown in Fig. 4. There are several occasions when the effect of rain on insects could be studied. We tried to exclude study periods overlapping with dawn and dusk rush hours, since the population was changing very rapidly during such events.

The first rain occurred in the late hours of July 9 (see Figs. 4, 6, 10). We show, in Fig. 11, how the counts of raindrops (blue curve) relate to the count of insects (red curve). We restrict the observation range to the first 200 m, to avoid closely spaced raindrops to be confounded with an insect at far distances, where the range resolution is strongly reduced. The separation has been done on the temporal duration of the signals, as described in connection with Fig. 9, but now adopting a threshold of 8 ms. We note that the rainfall evaluated from the lidar recordings is consistent with the measured values from the mechanical gauge. This supports the validity of our evaluation approach, which gives a much higher temporal resolution. Prominent insect count peaks occur at the beginning of the showers. The data are interpreted as the wash out of many insects, flying at high altitudes, even km, due to the falling raindrops already

at the early part of the rainfall. Only a small number of insects are observed to be still in the air during the ongoing rainfall. This convincingly shows that our method is able to separate insects from raindrops. Similar high-insect counts at the beginning of a rain shower have been observed with entomological radar techniques with observation of aggregations of insects at the front of a storm [4].

Since data on depolarization behavior of the echoes are not obtained with our setup, we also used the different depolarization properties between insects and raindrops to obtain an independent discrimination. We show, in Fig. 12, data during 1.5 h where transit time data as well as data in the depolarized light channel have been used. We note that while some deviations are observed, the data are largely congruent, and again exhibit a strong peak in insect abundance at the onset of rainfall.

We also looked at the influence of rainfall on insects of different size the same time period during the night of July 10, when three periods of rainfall occurred. We noted a tendency that smaller insects (with less intense echoes) occur somewhat before larger ones (with more intense

**Fig. 8** High temporal resolution recordings of two *insect* passages, with co- and depolarized signals displayed. The FFTs of the signals are also included

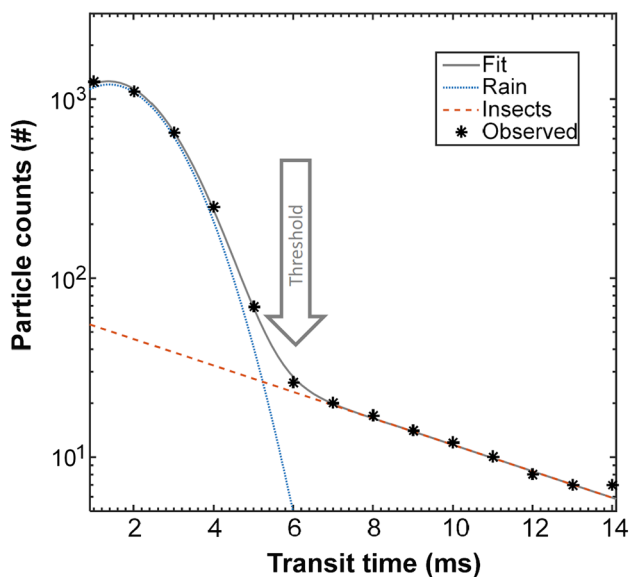
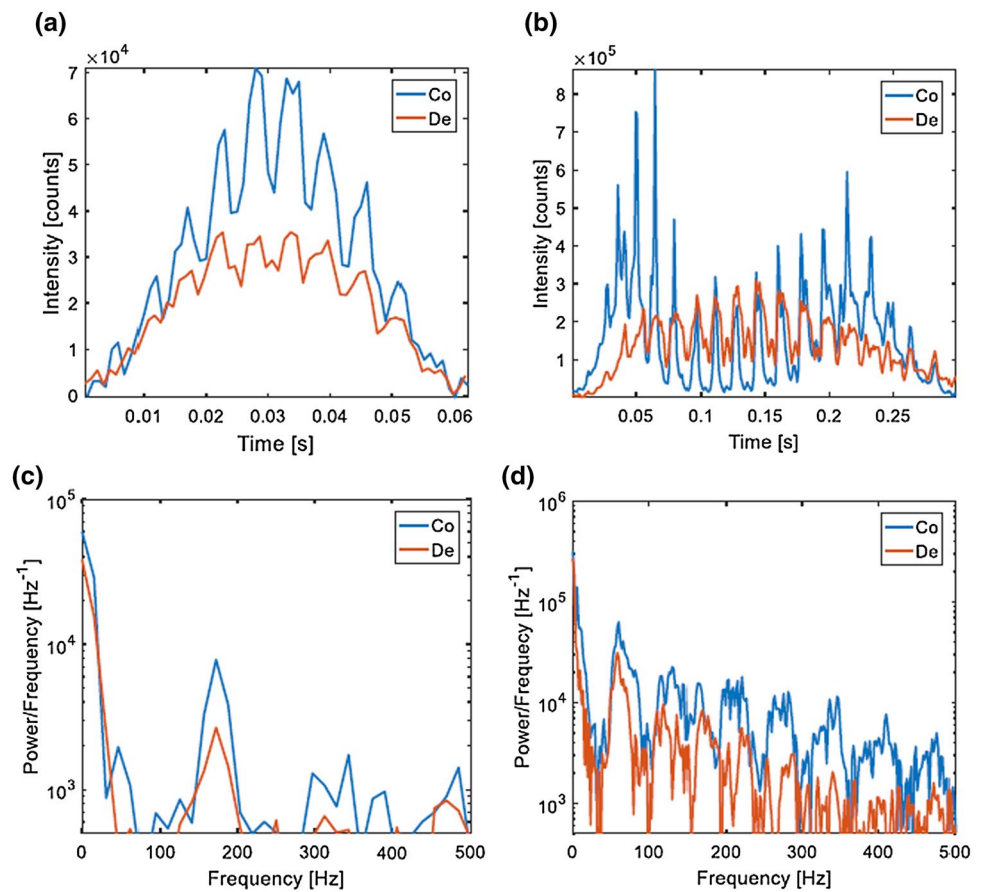


**Fig. 9** Histogram of particle counts with a particular beam transit time (1 ms bins). Short transit times correspond to raindrops, while longer times correspond to flying *insects*

echoes) at the beginning of rainfall, which might be related to smaller insects being more sensitive to rain than larger ones. However, at the present stage the result is not conclusive, since details in the range-dependent factors must be fully considered.

#### 4 Discussion and conclusions

Our long-term lidar observations, carried out in the rice fields, observed higher insect counts during nighttime than during daytime. This pattern could be caused by differing noise levels during day and night, but is consistent with other studies. In addition, most pest insects trapped during the lidar observations, such as *Chilo. suppressalis*, *Nilaparvata lugens* and *Nephotettix bipunctatus*, are nocturnal insects, and rice is not attractive to diurnal pollinators, such as bees, butterflies and flies.

Two peaks of flight activities at dusk and dawn, respectively, were observed every day with the CW lidar in a static horizontally sampling mode. Such so-called



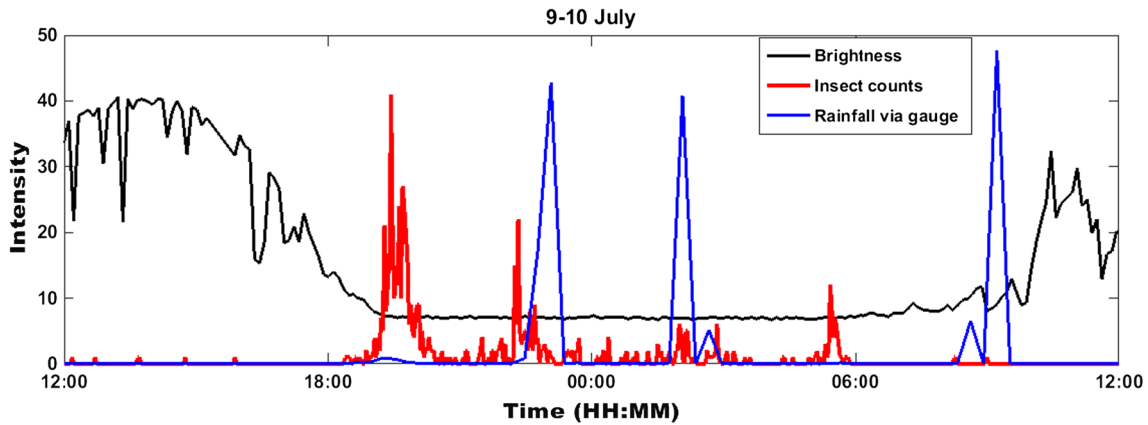


**Fig. 10** Twenty-four hours of atmospheric activity featuring the temporal distribution of flying fauna (shown in red). Signals due to raindrops have been suppressed using image erosion, relying on the considerably shorter beam transit time of raindrops compared to aero fauna. Rush hours at dusk and dawn are evident. The background

level is indicated in black, and the rainfall in blue, as measured at 5 min intervals with a mechanical gauge. Since several curves are shown with regard to their dynamic behavior, the y-axis is for simplicity labeled “Intensity”

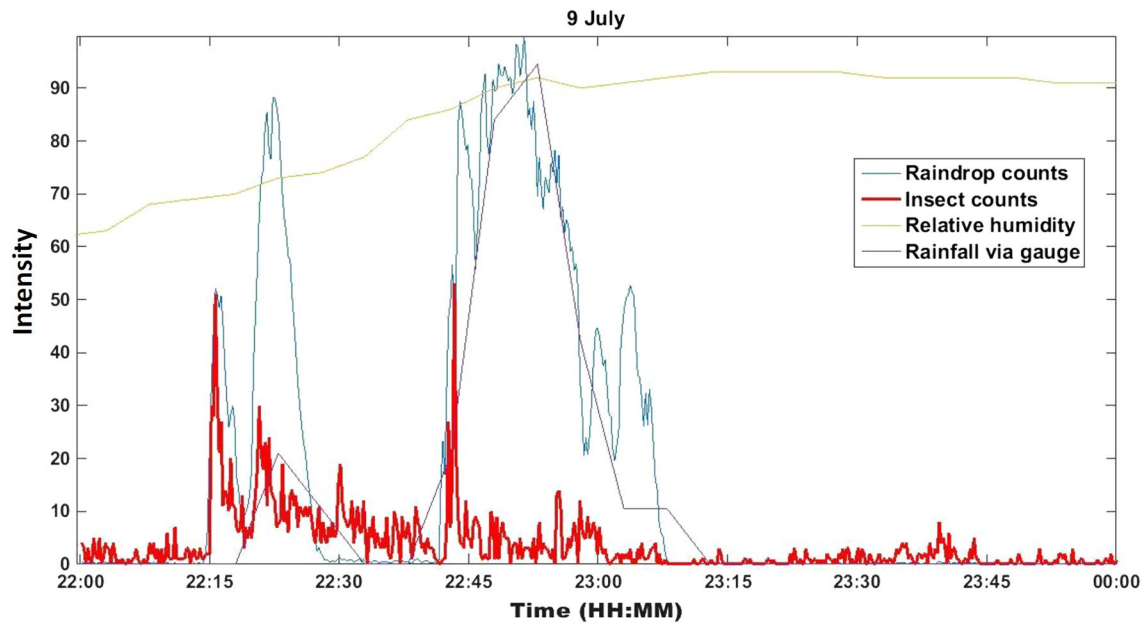


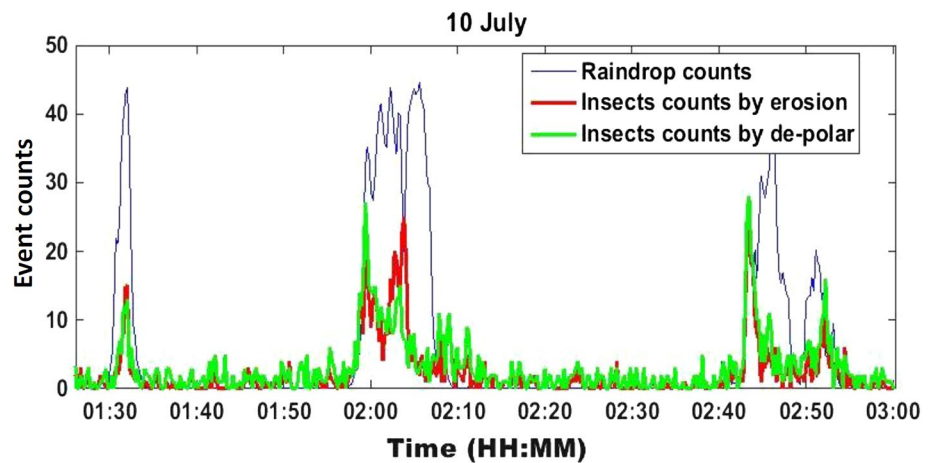
**Fig. 11** Insect counts (red) recorded in conjunction with raindrop counts (blue) show that insect events peak at the beginning of a rain shower. The interpretation is that high-flying insects are pushed

downwards to the ground by the rain. Since many curves are shown with regard to their dynamic behavior, the y-axis is for simplicity labeled “Intensity”

*crepuscular* activity peaks were in general always prominent in similar lidar experiments we have carried out. This phenomenon is also in accordance with the flight behavior of nocturnal migrant insects observed with entomological radars. According to early radar observations, migrant insects take off at dusk, and peak insect density is generally observed half an hour later [23–26]. The peak of insect density may last 1 or 2 h and then decreases to a low level after the insects have migrated [23–25]. If there were migrating

insects flying over the radar site through the whole night, the insect density would not decrease after dusk takeoff [25, 26]. The nocturnal migrant insects generally cease flying before dawn and form a sudden drop in insect density just before dawn [26, 27]. A weak peak of insect density related to landing of nocturnal insects or takeoff of diurnal insects is often observed at dawn [25]. In case of migration, the dusk peak is generally strong but the dawn peak is weak or absent [25]. Our long-term lidar observations

**Fig. 12** Data recorded during 90 min when three periods of rainfall occurred. *Insect* counts, as evaluated by the transit time method or using the depolarization method, are shown, in *red* and *green*, respectively. We note a quite good congruence between the two methods



support such a scenario, but we also note that the occurrence of a strong dusk and a weaker dawn population peak is very common due to the presence of crepuscular insects in abundance.

The present study also observed that there were peaks of insect activities just before rainfall and especially at the early stage of rainfall. This is because the migrating insects may concentrate in the outflow of the storm, which has been observed repeatedly with entomological radars [5]. Early radar observations indicated that the migrating insects at high altitude could be washed down by rain causing the aerial insect density to vary abruptly [26]. Our present study suggested that the high-flying insects did land at the early stage of the rain and they were not able to take off again after the storm. This forced landing of emigrants may trap part of the emigrant pest population and cause local crop damage later. If this rain-induced landing occurs in an immigration region, the rain area may become a severely damaged region.

In conclusion, our measurements show that a low-cost CW lidar system of the type employed in the present studies can provide huge amounts of useful data on flying insects and, thus, can be very helpful in entomological studies, in particular related to the abatement of agricultural pests. Measurements of occurrence and identification related to wing-beat frequency and depolarization ratio could provide information difficult to attain in other ways. We will be working on the continued refinement of analysis methods to develop the methodologies reported into robust and fully operational approaches.

**Acknowledgements** The authors gratefully acknowledge the support of Prof. Sailing He and Prof. Susanne Åkesson. We also thank Prof. Dunsong Li, Prof. Baoxin Zhang and Dirong Lai for assistance in the field. This work was financially supported by a Guangdong Province Innovation Research Team Program (No. 201001D0104799318), Henan Provincial Program for Innovative Talents of Science and Technology (No. 164200510015), the Swedish

Research Council, Lund Laser Centre, Centre for Animal Movement Research and Lund University.

**Open Access** This article is distributed under the terms of the Creative Commons Attribution 4.0 International License (<http://creativecommons.org/licenses/by/4.0/>), which permits unrestricted use, distribution, and reproduction in any medium, provided you give appropriate credit to the original author(s) and the source, provide a link to the Creative Commons license, and indicate if changes were made.

## References

1. T. Alerstam, J. Backman, G.A. Gudmundsson, A. Hedenström, S.S. Henningson, H. Karlsson, M. Rosen, R. Strandberg, A polar system of Intercontinental bird migration. *Proc. R. Soc. B* **274**(1625), 2523–2530 (2007)
2. V.A. Drake, H.K. Wang, I.T. Harman, Insect monitoring radar: remote and network operation. *Comput. Electron. Agric.* **35**, 77–94 (2002)
3. J.W. Chapman, D.R. Reynolds, A.D. Smith, Vertical-looking radar: a new tool for monitoring high-altitude insect migration. *Bioscience* **53**, 503–511 (2003)
4. H.Q. Feng, Radar entomology: 40 years of research - review and future aspect. *Henan Agric. Sci.* **9**, 121 (2009). (in Chinese)
5. V.A. Drake, D.R. Reynolds, *Radar entomology: observing insect flight and migration* (CABI, Wallingford, 2012)
6. J.A. Shaw, N.L. Seldomridge, D.L. Dunkle, P.W. Nugent, L.H. Spangler, J.J. Bromenshenk, C.B. Henderson, J.H. Churnside, J.J. Wilson, Polarization lidar measurements of honey bees in flight for locating land mines. *Opt. Express* **13**, 5853 (2005)
7. E.S. Carlsten, G.R. Wicks, K.S. Repasky, J.L. Carlsten, J.J. Bromenshenk, C.B. Henderson, Field demonstration of a scanning lidar and detection algorithm for spatially mapping honeybees for biological detection of land mines. *Appl. Opt.* **50**, 2112 (2011)
8. M. Brydegaard, Z.G. Guan, M. Wellenreuther, S. Svanberg, Fluorescence LIDAR imaging of insects - feasibility study. *Appl. Opt.* **48**, 5677 (2009)
9. Z.G. Guan, M. Brydegaard, P. Lundin, M. Wellenreuther, E. Svensson, S. Svanberg, Insect monitoring with fluorescence LIDAR techniques - field experiments. *Appl. Opt.* **48**, 5668 (2010)

10. L. Mei, Z.G. Guan, H.J. Zhou, J. Lv, Z.R. Zhu, J.A. Cheng, F.J. Chen, C. Löfstedt, S. Svanberg, G. Somesfalean, Agricultural pest monitoring using fluorescence lidar techniques. *Appl. Phys. B* **106**, 733 (2012)
11. M. Brydegaard, A. Gebru, S. Svanberg, Super resolution laser radar with blinking atmospheric particles - application to interacting flying insects. *Progress Electromagn. Res.* **147**, 141 (2014)
12. A. Runemark, M. Wellenreuther, H. Jayaweera, S. Svanberg, M. Brydegaard, Rare events in remote dark field spectroscopy: an ecological case study of insects. *IEEE JSTQE* **18**, 1573 (2012)
13. Y.Y. Li, H. Zhang, Z. Duan, M. Lian, G.Y. Zhao, X.H. Sun, J.D. Hu, L.N. Gao, H.Q. Feng, S. Svanberg, Optical characterization of agricultural pest insects: a methodological study in the spectral and time domains. *Appl. Phys. B* (2016). doi:[10.1007/s00340-016-6485-x](https://doi.org/10.1007/s00340-016-6485-x)
14. S.M. Zhu, Y.Y. Li, N.L. Gao, T.Q. Li, G.Y. Zhao, S. Svanberg, C.H. Lu, J.D. Hu, J.R. Huang, H.Q. Feng, Optical remote detection of flying Chinese agricultural pest insects using dark-field reflectance measurements. *Acta Entomol. Sin.* **59**, 1376 (2016)
15. Th. Scheimpflug, Improved method and apparatus for the systematic alteration or distortion of plane pictures and images by means of lenses and mirrors for photography and for other purposes. GB Patent No. 1196 (1904). <http://www.trenholm.org/hmmerk/TSBP.pdf>. Accessed 1 Mar 2017
16. G.Y. Zhao et al., CW polarization sensitive Scheimpflug lidar system, to appear (2017)
17. M. Brydegaard, Towards quantitative optical cross sections in entomological laser radar - potential of temporal and spherical parameterizations for identifying atmospheric fauna. *PLoS One* **10**(8), e0135231 (2015). doi:[10.1371/journal.pone.0135231](https://doi.org/10.1371/journal.pone.0135231)
18. H.M. Merklinger, *Focusing the view camera* (Dartmouth, Hanover, 2010)
19. L. Mei, M. Brydegaard, Atmospheric aerosol monitoring by an elastic Scheimpflug lidar system. *Opt. Express* **23**, 1613 (2015)
20. A. Gebru, M. Brydegaard, E. Rohwer, P. Neethling, Probing insect backscatter cross-section and melanization using kHz optical remote detection system. *SPIE J. Appl. Remote Sens.* **16611P** (2016)
21. E. Malmqvist, S. Jansson, S. Török, M. Brydegaard, Effective parameterization of laser radar observations of atmospheric fauna. *IEEE JSTQE* **22** (2016). doi:[10.1109/JSTQE.2015.2506616](https://doi.org/10.1109/JSTQE.2015.2506616)
22. L. Mei, M. Brydegaard, Continuous-wave differential absorption lidar. *Laser Photon. Rev.* **9**, 629–636 (2015)
23. H.Q. Feng, K.M. Wu, D.F. Cheng, Y.Y. Guo, Radar observations of the autumn migration of the beet armyworm *Spodoptera exigua* (*Lepidoptera: Noctuidae*) and other moths in northern China. *Bull. Entomol. Res.* **93**, 115–124 (2003)
24. H.Q. Feng, K.M. Wu, D.F. Cheng, Y.Y. Guo, Northward migration of *Helicoverpa armigera* (*Lepidoptera: Noctuidae*) and other moths in early summer observed with radar in northern China. *J. Econ. Entomol.* **97**, 1874–1883 (2004)
25. H.Q. Feng, K.M. Wu, D.F. Cheng, Y.Y. Guo, Spring migration and summer dispersal of *Loxostege sticticalis* (*Lepidoptera: Pyralidae*) and other insects observed with radar in northern China. *Environ. Entomol.* **33**, 1253–1265 (2004)
26. H.Q. Feng, K.M. Wu, Y.X. Ni, D.F. Cheng, Y.-Y. Guo, High-altitude windborne transport of *Helicoverpa armigera* (*Lepidoptera: Noctuidae*) and other moths in mid-summer in northern China. *J. Insect. Behav.* **18**, 335–350 (2005)
27. H.Q. Feng, K.M. Wu, Y.X. Ni, D.F. Cheng, Y.Y. Guo, Return migration of *Helicoverpa armigera* (*Lepidoptera: Noctuidae*) during autumn in northern China. *Bull. Entomol. Res.* **95**, 361–370 (2005)